MD Simulation of LNA-Modified Human Telomeric G-quadruplexes: A Free Energy Calculation

ARTICLE *in* MEDICINAL CHEMISTRY RESEARCH · JULY 2014

Impact Factor: 1.4 · DOI: 10.1007/s00044-014-1182-y

3 AUTHORS:

Amit Kumar Chaubey

Deen Dayal Upadhyaya Gorakhpur University

7 PUBLICATIONS **24** CITATIONS

SEE PROFILE

Kshatresh Dutta Dubey

Hebrew University of Jerusalem

14 PUBLICATIONS **59** CITATIONS

SEE PROFILE

Rajendra Prasad Ojha

Deen Dayal Upadhyaya Gorakhpur University

156 PUBLICATIONS **685** CITATIONS

SEE PROFILE

Med Chem Res
DOI 10.1007/s00044-014-1182-y

MEDICINAL CHEMISTRY RESEARCH

ORIGINAL RESEARCH

MD simulation of LNA-modified human telomeric G-quadruplexes: a free energy calculation

Amit Kumar Chaubey · Kshatresh Dutta Dubey · Rajendra Prasad Ojha

Received: 15 February 2014 / Accepted: 9 July 2014

Abstract One of the principal tools in the theoretical study of biological molecules is the method of molecular dynamic simulation. MD simulations have provided detailed information on the fluctuation and conformation changes of the system. It offers the prospects of detailed description of the dynamical structure with ion and water at molecular level. In this work, we have taken an oligomeric part of human telomeric DNA, d(TAGGGT), to form a tetrameric quadruplex structure and generate four modified complexes. For modification, we have taken locked nucleic acid. Here, we report the relative stability of these modified structures under K^+ ion conditions and binding interaction between the strands as determined by MD simulation followed by energy calculation. MM-PBSA method is performed for the determination of most stable complex. In free energy calculation, different strands are taken as the ligand and receptor. The energetic study shows that a modified quadruplex, in which first two modified strands are bind with other two unmodified strands, is more stable than other complexes. The formation and stabilization of these quadruplexes have been shown to inhibit the activity of telomerase, thus establishing telomeric quadruplex as an attractive target for cancer therapeutic intervention.

Keywords DNA · G-Quadruplex · LNA · MD simulation · Free-energy calculation

Introduction

Telomerase is a ribonucleoprotein at the ends of eukaryotic chromosomes that protect chromosome ends from fusion and is vital in safeguarding genomic stability. Single strands of telomeric DNA can adopt higher order structure, known as G-quadruplex, which involves in a wide range of biological and biochemical processes and holds significant promise as a pharmacological target. More details about quadruplexes can be found elsewhere (Blackburn, 1991; Sen and Gilbert, 1998). Fiber diffraction studies (Arnott *et al.*, 1974; Zimmerman *et al.*, 1975) and crystal structure (Kang *et al.*, 1992; Phillips *et al.*, 1997) demonstrate that such four-stranded structure are stabilized by stacked guanine tetrads (G-tetrads). The cyclic hydrogen bonding of four guanine bases forms G-tetrads in a coplanar arrangement. Cations also play a crucial role in stabilizing G-quartets by coordinating eight closely spaced guanine O6 atoms of successive G-tetrads, which form a twisted cube geometry. A variety of protein which can bind guanine-rich sequence and facilitate formation of G-quadruplex structure have now been identified (Walsh and Gualberto, 1992; Fang and Cech, 1993; Gu *et al.*, 1999) and further support the possible biological role for such structures. A growing number of groups are targeting G-quadruplex DNA with small molecules hoping to inhibit cancer growth; according to ligand-mediated stabilization of G-quadruplex, DNA might facilitate the regulation of gene expression and/or the inhibition of telomerase activity (Nathan, 2009). Since the telomerase is over expressed in the majority of malignant tumor cells and in relatively few

Electronic supplementary material The online version of this article (doi:10.1007/s00044-014-1182-y) contains supplementary material, which is available to authorized users.

A. K. Chaubey (✉) · K. D. Dubey · R. P. Ojha (✉)
Biophysics Unit, Department of Physics, DDU Gorakhpur University, Gorakhpur 273009, U.P, India
e-mail: amit.chb@gmail.com

R. P. Ojha
e-mail: rp_ojha@yahoo.com

Published online: 23 July 2014

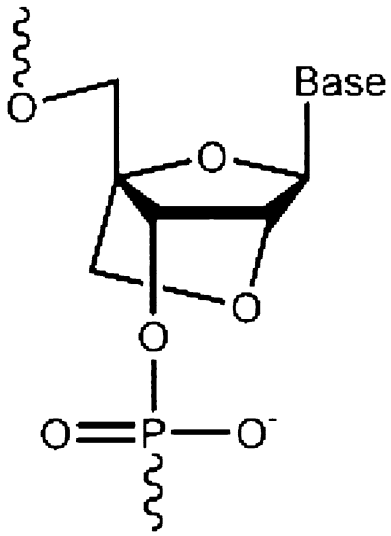

Fig. 1 Chemical structure of locked nucleic acid, in which a methylene bridge connecting the O2′ atom with C4′ atom locks the ribose ring

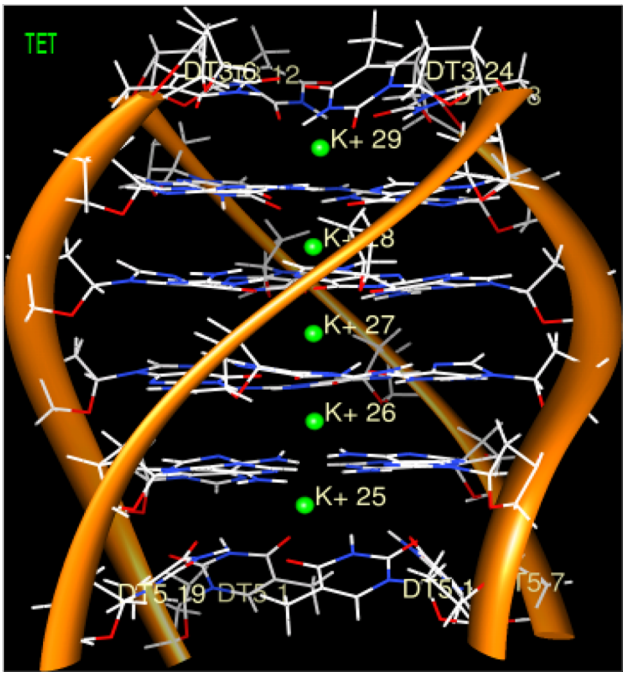

Fig. 2 Initial structure which has been taken as an oligomeric part of human telomeric DNA, d(TAGGGT) to form a parallel quadruplex structure d(TAGGGT)$_4$ (Color figure online)

somatic cells (Kim *et al.*, 1994), it is widely recognized as potential cancer-specific target (Patel and Phan, 2007; Organisian and Bryan, 2007; Mergny *et al.*, 2002; Cuesta *et al.*, 2003; De Cian *et al.*, 2008; Shammas *et al.*, 2004). The stabilization of G-qadruplex structures, when applied to cells, can inhibit apoptosis or replicative senescence (Ren and Chaires, 1999; Mikami-Terao *et al.*, 2008; Grand *et al.*, 2002). A large number of quadruplex ligands have been reported in the literature (Nathan, 2009; Neidle and Parkinson, 2008; Arora and Maiti, 2008; Dai *et al.*, 2008; Tan *et al.*, 2008; Ou *et al.*, 2008; Monchaud and Teulade-Fichou, 2008). In the early days of antisense research, several researchers (White *et al.*, 1996; Burgess *et al.*, 1995; Wang *et al.*, 1998) noted that the biological activities of certain oligonucleotides were not due to the true antisense effect, but rather were linked to the presence of contiguous guanines and the properties of the oligonucleotides to form quadruplex structures containing G-quartets.

Nucleic acid is central to transmission, expression, and conservation of genetic information. Consequently, high-affinity binding of complimentary nucleic acids has applications in biotechnology and medicine. In this context, the developments of nucleic acid with chemical modification rendering them high affinity and stability, since unmodified DNA or RNA oligonucleotides, have moderate affinities for complementary targets and low stability in biological fluids (Crooke, 2004). One such modification result is a locked nucleic acid (LNA) molecule (Fig. 1).

In this study, we decided to investigate the stability and existence of LNA-modified quadruplex structure with potassium ion. The stability of the hybridized structure of modified oligonucleotide with DNA oligonucleotide will also be studied. The potential of high-affinity hybridization by LNAs and LNA–DNA chimera might allow them to be effective inhibitors of telomerase. Here, we test this hypothesis and determine how high-affinity binding, the ratio of DNA and LNA oligomer, effects the formation of stable quadruplexes and, hence, as effect inhibitor. We have used molecular modeling method to build models of G-quadruplex arrays of tetrameric structure formed from extended human telomeric DNA. Since different reports have suggested variable conformation of human telomeric quadruplex in the presence of K^+ ions (Pradhan *et al.*, 2011) therefore, we used an unmodified and four hybridized structures with modified tetrameric d(TAGGGT)$_4$ quadruplex for simulation studies to understand their relative stabilities and interaction between the strands. Furthermore, to characterize the more energetically favorable quadruplex structure, we have estimated the binding free energy and entropy. This study provides detailed insight into the LNA-modified tetrameric quadruplex structures.

Materials and methods

Model and force field parameter generation

The initial structure has been taken as an oligomeric part of human telomeric DNA, d(TAGGGT) to form a parallel quadrulex structure d(TAGGGT)$_4$ (Fig. 2). It contains

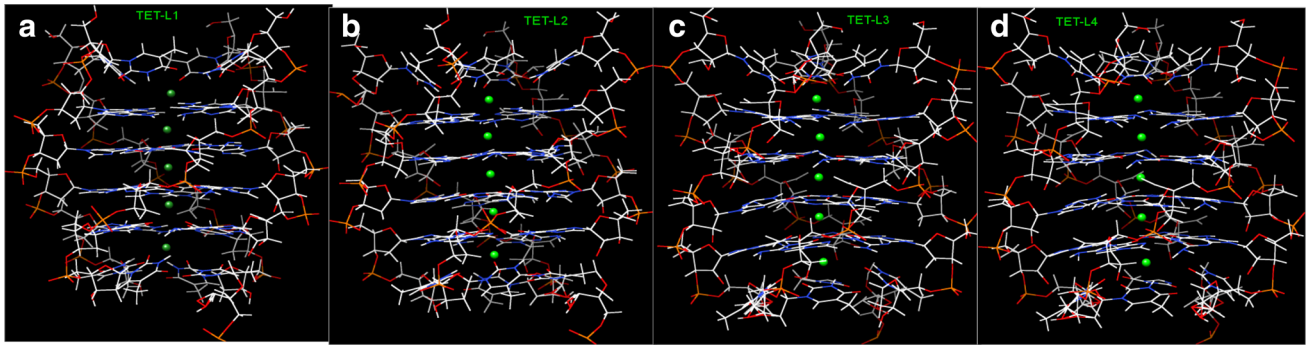

Fig. 3 All modified Quadruplex structures-**a** TET-L1: single-strand modified structure, **b** TET-L2: a mixed structure where first two strands are modified, **c** TET-L3: modification in first three strands and **d** TET-L4: all-strand modified structure (Color figure online)

three stacks of G-tetrads. Now, we have generated four hybridized (LNA–DNA) quadruplex structures (Fig. 3), where LNA was considered for modification. For modification, all the nucleotides in modified strand have been changed into LNA. In all five generated structures, TET is the initial (unmodified) structure (Fig. 2), and rest of the models are partially modified or modified (Fig. 3). In TET-L1 model, all nucleotides in strand 1 are modified with LNA. In TET-L2 model, first two strands are modified. There are first three strands that are modified in TET-L3 and in TET-L4 model, and all the nucleotides in strands are modified. Summary of model names, their modified and unmodified sequences, and production time are listed in Table 1.

Since the force field parameters for the modified nucleotides (LNA) are not available in literature, therefore, their parameters are generated using the GAUSSIAN 03 and RESP (Cornell *et al.*, 1995) program of AMBER 11. All the ab initio calculations are done at the DFT (B3LYP) level of theory with G-31G (d) basis set, using GAUSSIAN suite. Three-letter codes for all the fitted nucleosides were developed to standardize the naming of the modified nucleosides in pdb files. The parameters for the modified nucleotides are available as supplementary material (Table S1).

The nomenclature of the modified nucleotides used in the text is as follows.

Modified adenine: LCA,
Modified guanine: LCG, and
Modified thymine: TL5 and TL3,

where thymine is the ending nucleotide in all quadruplexes.

MD simulation and equilibration

The X-ray structure shows a vertical alignment of consecutive K^+ ions along the axis within the central core of the structure, in the middle between the G-tetrads. Thus, the ions were retained in the positions as observed in the crystal structure (Parkinson *et al.*, 2002). We placed 5 K^+ ions to the central channel of all the models manually. The models were solvated in a periodic TIP3P water box (Price and Brooks, 2004) at least 10 Å from any solute atom. Additional positively charged K^+ counter ions were included in the system to neutralize the charge on the DNA backbone. We have used recent amber force field ff03 (Duan *et al.*, 2003; Lee and Duan, 2004; Yang *et al.*, 2006) for parameter generation.

The simulation protocols were consistent for all of the systems. The systems were annealed from 0 to 300 K for 600 ps with continuous decrease of restrain (force constant was decreased from 100 to 5 kcal/molÅ^2 in six steps). The final stage of equilibration involved up to 1,200 ps runs using a force constant of 2 kcal/molÅ^2 on the solute and inner ions to fix them during equilibration. The final production run was carried out without any restrain on the system for 20 ns, and coordinates were saved after every 10 ps for analysis of their trajectories.

All calculations were carried out with the SANDER module of AMBER 11 (Case *et al.*, 2005). Periodic boundary condition has been applied using the particle-mesh Ewald (PME) method to treat long-range electrostatics. Hydrogen bonds were constrained using SHAKE (Ryckaert *et al.*, 1977). A time step of 2 fs and a direct space non-bonded cutoff of 10 Å were used. The Langevin coupling with a collision frequency of 2.0 was used for temperature regulation. A constant pressure of 1 atm. has been attained with isotropic molecule-based scaling with a relaxation time of 2 ps. The trajectories were analyzed using the PTRAJ module available in the AMBER 11 and visualized by means of the CHIMERA program (Pettersen *et al.*, 2004).

MM-PBSA calculation

Free energy analysis was performed using the MM-PBSA (Molecular Mechanics Poisson-Boltzman, surface area)

Table 1 Summary of model names, sequence type (molecular description), and production time of LNA-modified human telomeric quadruplex structures

Model name	DNA-sequence (molecular description)	Production time (ns)
TET	5′-d$(TAGGGT)_4$-3′	20
TET-L1	5′-d$((TL5)(LCA)(LCG)_3(TL3))(TAGGGT)_3$-3′	20
TET-L2	5′-d$((TL5)(LCA)(LCG)_3(TL3))_2(TAGGGT)_2$-3′	20
TET-L3	5′-d$((TL5)(LCA)(LCG)_3(TL3))_3(TAGGGT)$-3′	20
TET-L4	5′-d$((TL5)(LCA)(LCG)_3(TL3))_4$-3′	20

(Gohlke and Case, 2004) module of AMBER 11. Prior to the analysis, all water molecules and K^+ ions were stripped from trajectory. Here, the total free energy of binding is expressed as the sum of the contribution from the gas phase and solvation energy and an additional term of solute entropy. This can be expressed by the following equation:

$$\Delta G_{\mathrm{TOT}} = \Delta E_{\mathrm{GAS}} + \Delta E_{\mathrm{SOLV}} - \mathrm{T}\Delta \mathrm{S},$$

where ΔE_{GAS} is the total gas-phase energy given by

$$\Delta E_{\mathrm{GAS}} = \Delta E_{\mathrm{INT}} + \Delta E_{\mathrm{VDW}} + \Delta E_{\mathrm{ELEC}}.$$

Here, ΔE_{INT} corresponds to bond, angle, and torsion terms in the molecular mechanical force field. ΔE_{VDW} is the total solvation energy (polar and nonpolar), and TΔS corresponds to solute entropy effect. The detail of these terms can be found in our publications (Dubey and Ojha, 2011; Chaubey *et al.*, 2012). Analysis is done for the last 8 ns (12–20 ns) trajectory of all the complexes. The snapshots for these quadruplex are extracted at intervals of 20 ps. Prior to the analysis, all water molecules and K^+ ions were stripped from the trajectory. Solvation free energy is computed as the sum of polar and nonpolar contributions using a continuum solvent representation.

The polar contribution is calculated by Molsurf, implemented in AMBER 11. The nonpolar solvent contribution is estimated from a SASA dependent term

$$\Delta E_{\mathrm{SNP}} = \gamma.\mathrm{SASA} + \beta,$$

where γ is set to 0.0072 kcal/Å^2 and β to 0. The calculation for solute entropy contribution is performed with the NMODE module in AMBER 11. The snapshots were minimized in the gas phase using the conjugate gradient method for 1,000 steps, using a distance-dependent dielectric of 4r (r is interatomic distance) and with a convergence criterion of 0.1 kcal/molÅ for the energy gradient.

Results and discussion

Dynamic structure

From MD simulation of parallel human telomeric quadruplex structure and its modified structures, there are a series of snapshot extorted at periodic intervals. During dynamics, different snapshots at interval of 5 ns at 10, 15, and 20 ns of TET-L2 are represented in Fig. 4, while other snapshots of TET, TET-L1, TET-L3, and TET-L4 for interval 10, 15, and 20 ns are shown in Fig. S1. It has been seen that the quadruplex structure may be seen, which intact over the entire course of the simulation. During MD simulation, hydrogen-bonding pattern is reasonably well maintained. The nucleotide unit, at both the 5′ and 3′ ends of the sequence as indicated by larger thermal parameters, exhibits a larger range of dynamical motion. The effect does not appear to be propagated to a significant extent into the interior of the structure. In the initial structure, the central core of the stacked tetraplex has a line of five potassium ions that are coincident with the helical axis. Here, the metal ions are bipyramidally coordinated by eight equidistant carbonyl oxygen atoms. However, some of the potassium ions that are within a tetraplex deviate from the symmetrical geometry. In the snapshots of TET, TET-L2, TET-L3, and TET-L4, there are two K^+ ions that form bipyramidal binding with the O6 atom of guanine bases and show symmetry, while in TET-L1 model, there are four K^+ ions that form bipyramidal binding with the O6 atom of guanine bases, but those ions which lie outside of G-quartet in all the models move away from axis line.

The parallel three tetrads remain entirely stable with two cations in the channel, confirming that they are capable of achieving smooth equilibrium exchange of cations with the bulk solvent, which is experimentally observed on the hundreds of microsecond to millisecond time scale for the central ions (Hud *et al.*, 1999). The rigidity of the quadruplex is immediately lost in the absence of ions in the channel (Spackova *et al.*, 1999; Chowdhury and Bansal, 2001; Cavallari *et al.*, 2006).

In the initial stage of simulation, the ions are slightly displaced toward outside in unmodified structure, and there are only two ions that are bound in between the planes of quartet. In the first hybridizes structure (TET-L1), there are three ions present, in which two are bound in between the planes of quartet and the third one is slightly displaced from the axis of quartet (Fig. S1). However, after a long simulation (20 ns), there are only two ions bound between the three planes of quartet in all other structures, which shows the stability and occurrence of these structures. Since the

potassium–potassium, repulsion maybe partially shielded throughout the structure by the partial electronegative charges of the coordinating carbonyl group, which may be as great as half a charge (Jr Mackerell *et al.*, 1995).

Structural stability of the model

The root-mean-square deviation (rmsd) over the course of the simulation can be used as a measure of the conformational stability of a structure or model during the simulation. Here, we are interested in examining the conformational stability and dynamic effect of unmodified G-quadruplex structure from telomer DNA and compare with its modified complexes. The rmsds for TET-L2 and rest of the models over the course of simulation are presented in Figs. 5 and S2. Each plot (unmodified and modified) shows the rmsd from the all atom models (black color), backbone atoms (red color), base atoms (green), and middle base atoms (blue). A jump in the rmsd is observed within the first nanosecond, which is a consequence of relaxation of the starting model. All trajectories are stabilized during simulation with relatively small fluctuation in the models. As evident from the plot of modified structures, the rmsds of all atom models are higher than that of the backbone atoms, while in the plot of TET, the rmsds of backbone atoms are higher than that of all atoms. The rmsd of TET model is $\sim$2.9 Å for backbone atoms and $\sim$1.1 Å for base atoms, but it is not constant during simulation.

The rmsd of middle base atom is $\sim$0.6 Å and is almost constant during simulation period, which suggest that the tetrads formed by the quadruplex is intact, which forms a very stable structure. In TET-L2 structure, the rmsds of backbone atoms are $\sim$3.2 and $\sim$1.3 Å for base atoms, which gives constant fluctuations during 5–15 ns simulation (Fig. 5), while the rmsd corresponding to G-tetrads is $\sim$0.55 Å, varies in the same range, which again suggests a intact hybridized complex TET-L2. TET-L1 and TET-L4 give constant fluctuation during 7–14 and 5–20 ns simulation. The rmsd for the base atoms is $\sim$0.6 Å, while for the middle bases corresponding to tetrads, it is $\sim$0.5 Å. The rmsd of TET-L3 is not constant for base atom; it gives a large fluctuation of $\sim$3.2 Å after a simulation of 16 ns which is due to fraying of the end residue. The constant fluctuations in modified quadruplexes suggest the stability of structure. The backbone atoms are stabilized earlier during the simulation, and the higher rmsds of all atom models are the result of the wobbling effect of the nucleotide. All G-tetrads are held together in a coplanar array with eight hydrogen bonds which play a major role in ranking of these tetrads as most stable moieties in the models.

The RMSF (root-mean-square fluctuations) for five different quadruplexes are shown in Fig. 6. From the figure, it is clear that TET-L1 has the least atomic fluctuation during simulations relative to the other models. Except TET-L1, other models show similar type of atomic fluctuations for backbone and base atoms. From the plot, the base atoms show lower fluctuation, where C6 atom of guanine bases has lesser atomic fluctuation, shown by the lowest trough in the graph. The phosphate group of backbone in all nucleotides has larger atomic fluctuation which is shown by upper peaks in the graph of all models. The higher fluctuation corresponds to the end nucleoside (Thymidine) of all the strands. Among the purines, adenine shows higher fluctuation than the guanine bases, while all the guanines in the middle show lower fluctuation in the corresponding complex. It is because of the formation of hydrogen bonds in the tetrad, which is strongly bonded for the middle bases during the whole simulation period.

MM-PBSA calculation

Free energies calculated using MM-PBSA methodology can be used to study quadruplex models and provide a semiquantitative estimate of their stability (Stelf *et al.*, 2003; Agrawal *et al.*, 2008). The stability components of all structures are listed in Table 2. Although the energy values of the two different systems cannot be compared, the total binding energy E_{TOT} of the system for TET model is $-$3891.84 kcal/mol. The total binding energy ranged between $-$3133.82 and $-$3339.46 kcal/mol for all modified models. These values show that TET-L1 has the least favorable binding energy ($-$3133.82 kcal/mol), and TET model gives the most favorable binding energy ($-$3891.84 kcal/mol). Since all the models have sufficient negative binding energy, they show stability in their structure. These results are corroborated with the experimental results of the similar analog of the unmodified (Arnott *et al.*, 1974; Phillips *et al.*, 1997; Makarow *et al.*, 1997) and modified (Randazzo *et al.*, 2004; Sacca *et al.*, 2005) quadruplexes. The stability of hybridized oligonucleotide is also confirmed by its comparable energy values with the known stable complexes (Table 2). The total energy of the solute E_{GAS} includes the electrostatic energy, van der Waals energy derived from a Lennard-Jones potential, and the internal energy. Finite difference Poisson–Bolttzman equations were used to calculate the electrostatic potential field. The binding energy calculation for the quadruplex suggested a favorable contribution for van der Waals energy E_{VDW} for all quadruplex models.

The mechanism of preferential selection of strands in the formation of quadruplexes for the unmodified and modified quadruplexes can be understood by observing the free energy and its components for all structures. The binding free energy components for these quadruplexes are measured by MM-PBSA method and are shown in Table 3.

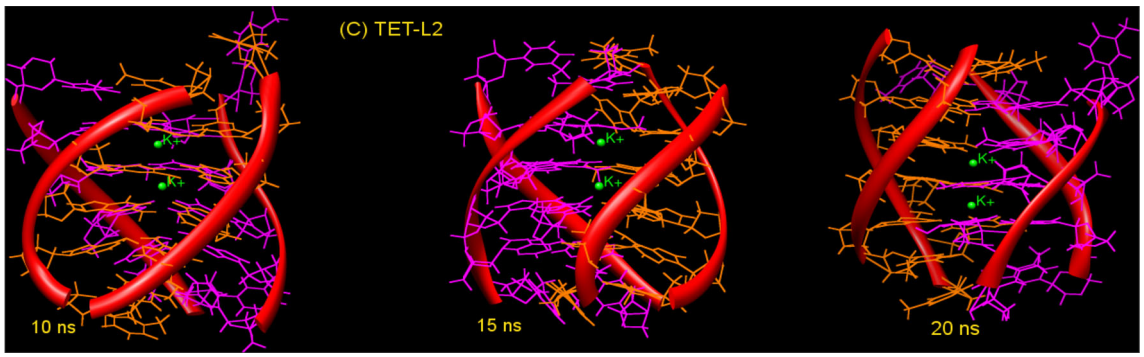

Fig. 4 Snapshots of the TET-L2 model, during production dynamics of 10, 15, and 20 ns. There are two ions bound in between the planes of quartet. In this model, unmodified strands are in *orange color*, while modified strands are in *magenta color*. K^+ ions present in central cavity are shown in *green* (Color figure online)

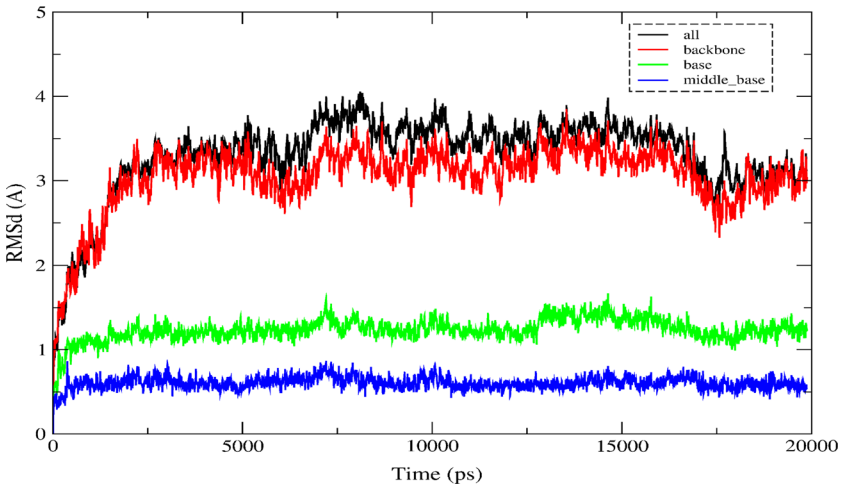

Fig. 5 RMSD plot showing the stability of TET-L2 model, during MD run. RMSD values calculated for all atoms (*black*), backbone-only atoms (*red*), base-only atoms (*green*), and middle base atoms (*blue*) (Color figure online)

For unmodified hybridized and fully modified complexes, all energy values are calculated for binding of each strand or a pair of strand with remaining part of the complex. The nonpolar contribution of the salvation energy can be calculated from the solvent-accessible surface area of the molecule. The binding free energy calculation for the quadruplex suggests a favorable contribution from solute electrostatic energy ΔE_{ELE} for all structures. In addition, a favorable contribution is also found for the van der Waals energy ΔE_{VDW}. Moreover, we observed unfavorable entropy contributions $T\Delta S$ for all models of quadruplex. The solute entropy term of binding for all five models ranged between −26.74 and −39.90 kcal/mol. The binding free energy ΔG_{TOT} of all five structures varies from 194.31 to −6.01 kcal/mol. These values show that TET-L2, in which two unmodified strands bind with other two modified strands, is more stable among other models, because it has the lowest binding free energy (−6.01 kcal/mol). The binding free energy values suggest that TET-L2 model exhibits higher stability than the other unmodified and modified structures.

Effect of G-quartet on binding energy

It has been observed that during simulation, some of the outer nucleotides show much fluctuation; therefore, the binding energies of the inner tetrads are also calculated and discussed (Table 4). The free energy calculation between the strands of inner tetrad, the electrostatic energy ΔE_{ELE} makes an unfavorable contribution and van der Waals energy ΔE_{VDW} provides favorable contribution. In addition, the total solvation energy ΔE_{SOLV} also contributes favorable to the total binding free energy. This implies that Van der Waal and solvation energy are important contributions to calculate the binding free energy of quadruplex. Moreover, we observed unfavorable entropic contribution for all quadruplex models. For inner tetrad, we have also calculated the binding free energy between the modified and unmodified strands (Table 4). There are three mixed hybridized structures in which modified and unmodified strands are bind together. Among these, the contribution of solute entropy varies from −3.72 to −11.60 kcal/mol, and the binding free energy ranged between −47.47 and

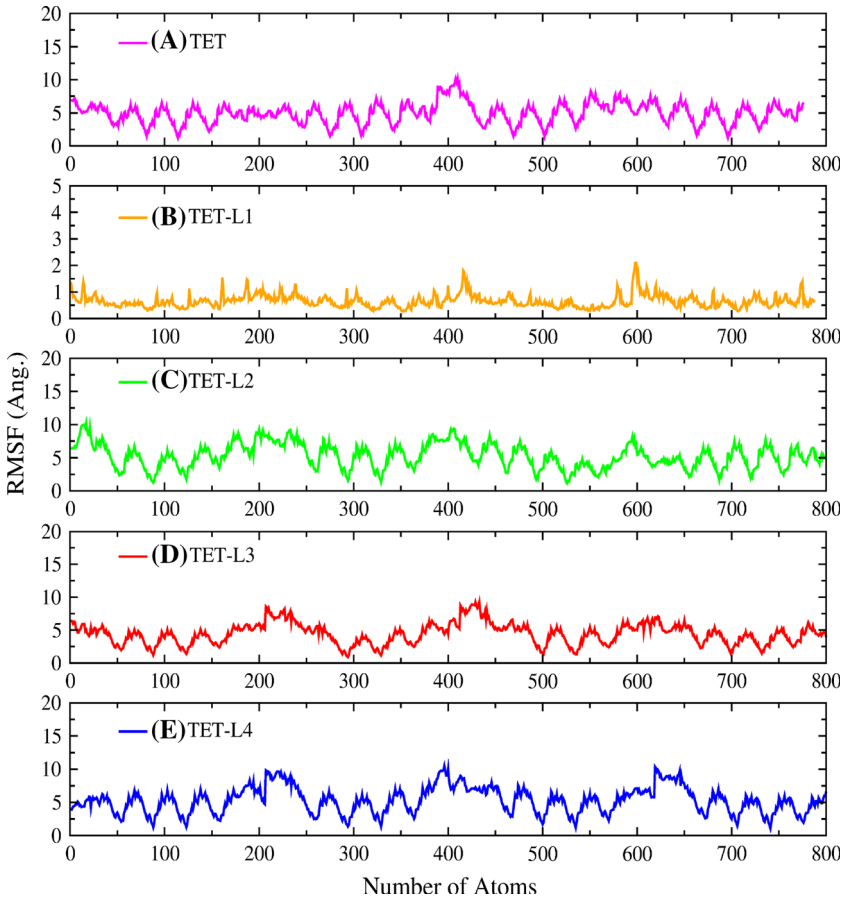

Fig. 6 Root-mean-square fluctuation versus atom number for all modified and unmodified modeled quadruplex structures during molecular dynamic simulation (Color figure online)

26.70 kcal/mol. The binding free energy between the tetrads of TET-L2, where two strands are modified, is more stable than others. Its lowest free energy (−47.47 kcal/mol) suggests that inner tetrads of TET-L2 exhibit better stability than the other modified structures.

These free energy calculations suggest a mechanism of the formation of quadruplexes of modified LNA, in which two strands combined together to form a dimer structure which can re-interact to form a quadruplex structure. Since the energy differences between these dimmers are comparable, therefore, their preference of interaction is not unidirectional. The two strands may combined together to form a Watson or Crick type of dimer which may remain in the presence of a suitable cation. These dimers re-interact with Crick or Watson type of dimer to form a quadruplex with Watson and Crick grooves. The possibility of formation of quadruplexes by the interaction of individual strand is also probable, but the probability of such complexes is very less. Similar is the case observed for the unmodified quadruplexes. However, the preferential selection of the strands in the formation of dimers may be different from the case of modified strands. It is to be noted that these interactions are favorable in the presence of suitable cations only, which stabilized the quadruplex structure by contributing electrostatic interaction with the O6 atoms of guanine bases.

Hydrogen-bonding patterns

The starting fiber model (3), as well as high-resolution crystal structure (6) of parallel quadruplex with coordinated cations, contains N1-H1–O6 and N2-H2–N7 (Hoogsteen type) hydrogen bonds between the adjacent guanines, leading to eight hydrogen bonds per G-tetrad. The ab initio study on G-tetrad (9) also suggested that, in the absence of a coordinated cation, G-tetrad is stabilized by bifurcated hydrogen bonds between N1-H1–O6 and N2-H2–O6 atoms, whereas MD simulation of the 4-mer parallel quadruplex structure without any coordinated cations (44) reported disruption of the G-tetrad geometry due to strand slippage. It is observed that during the molecular dynamics simulation, hydrogen-bonding scheme within a G-tetrad depends on the electrostatic interaction between the polar atoms of guanine bases and the coordinating molecules. The interatomic distances between potential hydrogen-bond-forming groups within a G-tetrad and

Table 2 Energy contributions for all the models (modified and unmodified parallel G-quadruplexes)

	TET	TET-L1	TET-L2	TET-L3	TET-L4
E_{ELE}	900.61 ± 45.30	1075.96 ± 59.60	654.62 ± 50.73	511.93 ± 64.67	519.73 ± 72.26
E_{VDW}	−279.58 ± 10.75	−264.60 ± 13.76	−227.04 ± 12.99	−203.90 ± 16.84	−200.27 ± 12.61
E_{INT}	1124.10 ± 20.15	1725.76 ± 17.22	1821.74 ± 24.09	1936.73 ± 22.70	2025.35 ± 23.13
E_{GAS}	1744.86 ± 44.55	2537.12 ± 65.89	2249.33 ± 48.18	2244.76 ± 59.94	2344.81 ± 68.55
E_{SNP}	29.64 ± 0.72	29.60 ± 0.69	33.35 ± 1.07	35.43 ± 1.11	36.69 ± 0.92
E_{SP}	−5666.34 ± 42.40	−5700.54 ± 51.98	−5610.25 ± 47.60	−5619.64 ± 113.44	−5629.08 ± 69.92
E_{SOLV}	−5636.70 ± 42.46	−5670.94 ± 51.73	−5576.89 ± 47.94	−5584.21 ± 113.35	−5592.39 ± 69.93
E_{TOT_ELE}	−4765.74 ± 25.12	−4624.58 ± 26.52	−4955.63 ± 20.14	−5107.71 ± 13.60	−5109.36 ± 104.44
E_{TOT}	**−3891.84 ± 27.16**	**−3133.82 ± 28.96**	**−3327.57 ± 24.06**	**−3339.46 ± 130.54**	**−3247.58 ± 101.25**

The change in total free energy is shown in bold to highlight the comparison of change in free energy in different conformations

E_{ELE} coulombic energy, E_{VDW} van der waals energy, E_{INT} internal energy, $E_{GAS} = E_{ELE} + E_{VDW} + E_{INT,}$ E_{SNP} nonpolar solvation energy, E_{SP} polar solvation energy, $E_{SOLV} = E_{SNP} + E_{SP}$ total solvation energy, $E_{TOT\_ELE} = E_{ELE} + E_{SP}$ total electrostatic energy, $E_{TOT} = E_{GAS} + E_{SOLV}$ total energy (enthalpy)

All energy values are in kcal/mol

Table 3 Comparison of the binding free energy between the strands of G-quadruplex structures

	TET	TET-L1	TET-L2	TET-L3	TET-L4
ΔE_{ELE}	1675.87 ± 38.48	1967.93 ± 37.60	1733.80 ± 29.03	1756.78 ± 36.35	1798.69 ± 36.31
ΔE_{VDW}	−67.76 ± 5.72	−57.77 ± 6.11	−38.99 ± 5.34	−63.99 ± 5.92	−52.14 ± 2.91
ΔE_{INT}	0	−149.89 ± 22.70	−135.12 ± 28.78	5.69 ± 2.31	0
ΔE_{GAS}	1608.12 ± 37.00	1760.27 ± 49.61	1559.69 ± 36.14	1698.48 ± 33.90	1746.54 ± 35.0
ΔE_{SNP}	−8.89 ± 0.57	−8.87 ± 0.54	−7.66 ± 0.47	−7.74 ± 0.65	−5.97 ± 0.33
ΔE_{SP}	−1515.60 ± 37.92	−1586.47 ± 40.18	−1584.79 ± 25.92	−1685.47 ± 117.51	−1660.24 ± 78.50
ΔE_{SOLV}	−1524.50 ± 38.00	−1595.34 ± 40.39	−1592.45 ± 26.14	−1693.21 ± 117.50	−1666.21 ± 78.37
ΔE_{TOT_ELE}	160.27 ± 24.17	381.46 ± 29.52	149.01 ± 13.87	71.31 ± 125.80	138.45 ± 97.53
$\Delta E_{GAS+SOLV}$	83.62 ± 21.07	164.93 ± 32.25	−32.75 ± 28.03	5.28 ± 125.33	80.34 ± 96.59
TΔS	−39.90	−29.38 ± 9.68	−26.74	−36.69 ± 9.65	−27.35
ΔG_{TOT}	**123.52**	**194.31**	**−6.01**	**41.97**	**107.69**

The change in total free energy is shown in bold to highlight the comparison of change in free energy in different conformations

ΔE_{ELE} coulombic energy, ΔE_{VDW} van der waals energy, ΔE_{INT} internal energy, $\Delta E_{GAS} = \Delta E_{ELE} + \Delta E_{VDW} + \Delta E_{INT,}$ ΔE_{SNP} nonpolar solvation energy, ΔE_{SP} polar solvation energy, $\Delta E_{SOLV} = \Delta E_{SNP} + \Delta E_{SP}$ total solvation energy, $\Delta E_{TOT\_ELE} = \Delta E_{ELE} + \Delta E_{SP}$ total electrostatic energy, $\Delta E_{GAS+SOLV} = \Delta E_{GAS} + \Delta E_{SOLV}$ enthalpy, $T\Delta S$ solute entropy, $\Delta G_{TOT} = \Delta E_{GAS+SOLV}$-$T\Delta S$ absolute free energy

All energy values are in kcal/mol

distances between different O6 atoms in the MD structures obtained during 20 ns dynamic run are listed in Table S2 for all other models.

During the simulation, standard Hoogsteen types N1-H1–O6 and N2-H2–N7 hydrogen bonds in all G-tetrads (Fig. 7 for TET-L2 and Fig. S3 for rest models) are retained for all quadruplex models. However, due to the strong attractive force between coordinated K^+ ion and O6 atoms, guanine bases in some G-tetrads undergo in-plane rotational motion. Because of this rotational motion, N1-H1–O6 and in some cases N2-H2–N7 hydrogen bonds are elongated, whereas N1 atom and N2 atom of guanine base come closer to N7 and O6 atom of neighboring guanine base and form N1-H1–N7 and N2-H2–O6 hydrogen bond. Thus, their centered hydrogen bond plays the additional role to stabilize these tetrads. From Table S2, G-tetrad of TET-L2 forms 31 hydrogen bonds, which is the maximum number of hydrogen bonds in comparison to all other models. Due to maximum number of hydrogen bonding between the tetrads, TET-L2 shows more stability.

It suggests that the hybridized structure has better stability than the corresponding fully modified and unmodified structure. Interestingly, such oligonucleotides are complementary to the RNA template component of human

Table 4 Comparison of the binding free energy between the modified and unmodified strands of inner G-tetrad of quadruplexes

	TET-L1	TET-L2	TET-L3
ΔE_{ELE}	249.84 ± 21.62	234.91 ± 12.79	188.90 ± 17.35
ΔE_{VDW}	−10.51 ± 2.07	−9.32 ± 2.77	−9.86 ± 2.51
ΔE_{INT}	−73.29 ± 7.61	−56.43 ± 16.75	−13.66 ± 15.32
ΔE_{GAS}	166.04 ± 14.76	169.15 ± 14.47	165.38 ± 21.96
ΔE_{SNP}	−3.03 ± 0.13	−2.79 ± 0.12	−2.63 ± 0.21
ΔE_{SP}	−145.67 ± 54.29	−224.24 ± 8.39	−147.64 ± 39.88
ΔE_{SOLV}	−148.69 ± 54.27	−227.03 ± 8.44	−150.28 ± 39.93
ΔE_{TOT_ELE}	104.18 ± 46.65	10.67 ± 11.15	41.26 ± 32.03
$\Delta E_{GAS+SOLV}$	17.35 ± 48.15	−57.88 ± 16.65	15.10 ± 43.42
TΔS	−3.72 ± 8.22	−10.41 ± 7.62	−11.61 ± 8.10
ΔG_{TOT}	**21.07**	**−47.47**	**26.70**

The change in total free energy is shown in bold to highlight the comparison of change in free energy in different conformations

ΔE_{ELE} coulombic energy, ΔE_{VDW} van der waals energy, ΔE_{INT} internal energy, $\Delta E_{GAS} = \Delta E_{ELE} + \Delta E_{VDW} + \Delta E_{INT,}$ ΔE_{SNP} nonpolar solvation energy, ΔE_{SP} polar solvation energy, $\Delta E_{SOLV} = \Delta E_{SNP} + \Delta E_{SP}$ total solvation energy, $\Delta E_{TOT\_ELE} = \Delta E_{ELE} + \Delta E_{SP}$ total electrostatic energy, $\Delta E_{GAS+SOLV} = \Delta E_{GAS} + \Delta E_{SOLV}$ enthalpy, $T\Delta S$ solute entropy, $\Delta G_{TOT} = \Delta E_{GAS+SOLV}\text{-}T\Delta S$ absolute free energy

All energy values are in kcal/mol

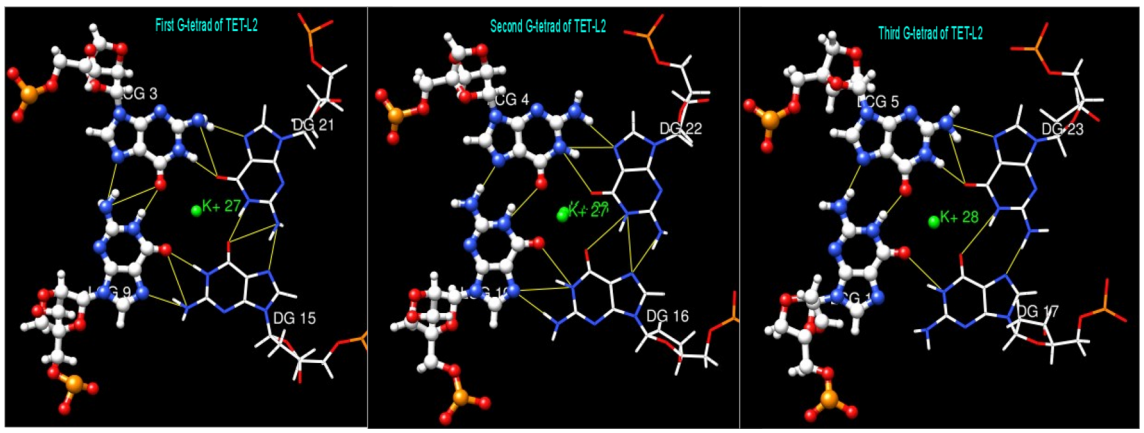

Fig. 7 Hydrogen-bonding pattern between the atoms of first, second, and third G-tetrad of TET-L2 model (Color figure online)

telomerase, which act as potent and selective inhibitor with IC_{50} values as low as 10 nM (Elayadi *et al.*, 2002). Therefore, the oligonucleotide modified with LNA and complementary to RNA template having G-rich sequences may be proved as a better inhibitor of telomerase activity. While these short LNAs are complementary to many sequences within the genome, there is no obvious toxicity to all after transfections (Elayadi *et al.*, 2002). We anticipate that LNAs will prove to be an important addition to the chemical repertoire for nucleic acid recognition with this mechanism and its action.

Conclusions

In this work, we have done MD simulation to understand in detail the structural stability, dynamics, binding free energy, and the role of hydrogen bonding of human telomeric DNA, $d(TAGGGT)_4$ structure. The structures are modified with LNA. The binding free energy calculations show the stability of all modified complexes, and it explains the understanding of interactions between the strands to form a stable quadruplex structure. The results from free energy calculation suggest that a modified complex, where two modified strands are bind with other two unmodified strands, is more stable than other complexes. Therefore, the G-rich sequences for the modified and unmodified oligonucleotides first form the Watson and Crick type of dimer. These two dimers re-interact to form a complex, known as quadruplex which contains two Watson and two Crick types of groove. Interestingly, these interactions take place in the presence of cation. These cations are responsible to keep intact the dimers as well as tetramers, and hence trust worthy for the stability of

quadruplexes. This study suggests that LNA-modified oligonucleotide can form a stable hybridized structure and may play a role in inhibition of telomerase activity. The tendency of human telomeric G-quadruplex structure to adopt multiple conformations under varying environmental conditions poses a significant challenge in the appropriate design of conformation-specific drugs that could efficiently bind and stabilize the structure.

Therefore, these modified oligonucleotides may be able to stabilize the G-rich oligonucleotides in in vivo system, through the structural formation as discussed above. As a result, the further synthesis of the corresponding gene may be inhibited, and hence be able to stop the growth of the tumor or the cancerous cell. Such studies may be helpful for the researcher of other fields e.g., biochemistry, molecular biology, immunology, etc.

Acknowledgments The authors are thankful to DST, New Delhi for computational facility in the form of FIST scheme. A part of computational work is done on SCFBio, IIT, New Delhi. We thankfully acknowledge the partial computational work at BRAF of C-DAC, Pune, India.

References

Agrawal S, Ojha RP, Maiti S (2008) Energetics of the human tel-22 quadruplex telomestatin interaction: a molecular dynamics study. J Phys Chem B 112:6828–6836

Arnott S, Chandrasekaran R, Marttila CM (1974) Structures for polyinosinic acid and polyguanylic acid. Biochem J 141:537–543

Arora A, Maiti SJ (2008) Effect of loop orientation on quadruplex-TMPyP4 interaction. Phys Chem B 112:8151–8159

Blackburn EH (1991) Structure and function of telomers. Nature 350:569–573

Burgess TL, Fisher EF, Ross SL, Bready JV, Qian YX, Bayewitch LA et al (1995) The antiproliferative activity of c-myb and c-myc antisense oligonucleotides in smooth muscle cells is caused by a nonantisense mechanism. Proc Natl Acad Sci USA 92:4051–4055

Case DA, Cheathem TE et al (2005) The AMBER biomolecular simulation programs. J Comput Chem 26:1668–1688

Cavallari N, Calzolarii A, Garbesi A, Di Felice R (2006) Stability and migration of metal ions in G4-wires by molecular dynamics simulations. J Phys Chem B 110:26337–26348

Chaubey AK, Dubey KD, Ojha RP (2012) Stabilty and free energy calculation of LNA modified quadruplex: a molecular dynamics study. J Comput Aided Mol Des 26:289–299

Chowdhury S, Bansal M (2001) G-quadruplex structure can be stable with only some coordination sites being occupied by cations: a six-nanosecond molecular dynamics study. J Phys Chem B 105:7572–7578

Cornell WD, Cieplak P, Bayly CI, Gould IR Jr, Ferguson DM, Spellmeyer DC, Fox T, Caldwell JW, Kollman PA (1995) A second generation force field for the simulation of proteins, nucleic acids, and organic molecules. J Am Chem Soc 117:5179–5197

Crooke ST (2004) Progress in antisense technology. Annu Rev Med 55:61–95

Cuesta J, Read MA, Neidle S (2003) The design of G-quadruplex ligands as telomerase inhibitors. Mini Rev Med Chem 3:11–21

Dai JX, Carver M, Yang DZ (2008) Polymorphism of human telomeric quadruplex structures. Biochimie 90:1172–1183

De Cian A, Lacroix L, Douarre C, Temime-Smaali N, Trentesaux C, Riou JF, Mergny JL (2008) Targeting telomeres and telomerase. Biochimie 90:131–155

Duan Y, Wu C, Chowdhury S et al (2003) A point-charge force field for molecular mechanics simulations of proteins based on condensed-phase quantum mechanical calculations. J Comput Chem 24:1999–2012

Dubey KD, Ojha RP (2011) Binding free energy calculations with hybrid QM/MM methods for Abl kinase inhibitors. J Biol Phys 37:69–78

Elayadi AN, Braasch DA, Coret DR (2002) Implications of high affinity hybridization by locked nucleic acids for inhibition of human telomerase. Biochemistry 41:9973–9981

Fang G, Cech TR (1993) Characterization of a G-quartet formation reaction promoted by the beta-subunit of the Oxytricha telomere-binding protein. Biochemistry 32:11646–11657

Gohlke H, Case DA (2004) Converging free energy estimates: MM-PB(GB)SA studies on the protein–protein complex Ras–Raf. J Comput Chem 25:238–250

Grand CL, Han HY, Munoz RM, Weitman S, Von Hoff DD, Hurley LH, Bearss DJ (2002) The cationic porphyrin TMPyP4 down-regulates c-MYC and human telomerase reverse transcriptase expression and inhibits tumor growth in vivo. Mol Cancer Ther 1:565–573

Gu J, Leszczynski J, Bansal M (1999) A new insight into the structure and stability of Hoogsteen hydrogen-bonded G-tetrad: an ab initio SCF study. Chem Phys Lett 311:209

Hud NV, Schultze P, Sklenar V, Feigon J (1999) Localization of ammonium lon in the minor groove of DNA duplexes in solution and the origin of DNA A-tract bending. J Mol Biol 285:233–243

Jr Mackerell AD, Wiorkiewics-Kuczera J, Karplus MJ (1995) An all-atom empirical energy function for the simulation of nucleic acids. Am Chem Soc 117:11946–11975

Kang C, Zhang X, Ratliff R, Moyzis R, Rich A (1992) Crystal structure of four-stranded *Oxytricha telomeric* DNA. Nature 356:126–131

Kim NW et al (1994) Specific association of human telomerase activity with immortal cells and cancer. Science 266:2011–2015

Lee MC, Duan Y (2004) Distinguish protein decoys by using a scoring function based on a new AMBER force field, short molecular dynamics simulations, and the generalized born solvent model. Proteins 55:620–634

Makarow VL, Hirose Y, Langmore JP (1997) Long G tails at both ends of human chromosomes suggest a C strand degradation mechanism for telomere shortening. Cell 88:657–666

Mergny JL, Riou JF, Mailliet P, Teulade-Fichou MP, Gilson E (2002) Natural and pharmacological regulation of telomerase. Nucleic Acids Res 30:839–865

Mikami-Terao Y, Akiyama M, Yuza Y, Yanagisawa T, Yamada O, Yamada H (2008) Antitumor activity of G-quadruplex-interactive agent TMPyP4 in K562 leukemic cells. Cancer Lett 261:226–234

Monchaud D, Teulade-Fichou MP (2008) A hitchiker guide to G-quadruplex ligands. Org Biomol Chem 6:627–636

Nathan WL (2009) Targeting G-quadruplex DNA with small molecules. Chimia 63(3):134–139

Neidle S, Parkinson GN (2008) Quadruplex DNA crystal structures and drug design. Biochimie 90:1184–1196

Organisian L, Bryan TM (2007) Physiological relevance of telomeric G-quadruplex formation: a potential drug target. BioEssays 29:155–165

Ou TM, Lu YJ, Tan JH, Huang ZS, Wong KY, Gu LQ (2008) G-quadruplexes: targets in anticancer drug design. Chem Med Chem 3:690–713

Parkinson GN, Lee M, Neidle S (2002) Crystal structure of parallel quadruplexes from human telomeric DNA. Nature 417:876–880

Patel DJ, Phan AT (2007) Human telomere, oncogenic promoter and 50-UTR G-quadruplexes: diverse higher order DNA and RNA targets for cancer therapeutics. Nucleic Acids Res 35:7429–7455

Pettersen EF, Goddard TD, Huang CC, Couch GS et al (2004) UCSF chimera: a visualization system for exploratory research and analysis. J Comput Chem 25:1605–1612

Phillips K, Dauter Z, Murchie AIH, Lilley DMJ, Luisi BJ (1997) The crystal structure of a parallel-stranded guanine Tetraplex at 0.95 Å resolution. Mol Biol 273:171–182

Pradhan et al (2011) Selection of G-quadruplex folding topology with LNA-modified human telomeric sequences in K+ solution. Chem Eur J 17:2405–2413

Price DJ, Brooks CL 3rd (2004) A modified TIP3P water potential for simulation with Ewald summation. J Chem Phys 121: 10096–10103

Randazzo A, Esposito V, Ohlenschlager O, Ramachandran R, Mayol L (2004) NMR solution structure of a parallel LNA quadruplex. Nucleic Acids Res 32:3083–3092

Ren J, Chaires JB (1999) Sequence and structural selectivity of nucleic acid binding ligands. Biochemistry 38:16067–16075

Ryckaert JP, Ciccotti G, Berendsen HJC (1977) Numerical integration of the cartesian equations of motion of a system with constraints: molecular dynamics of n-alkanes. J Comput Phys 23:327–341

Sacca B, Lacroix L, Mergny JL (2005) The effect of chemical modifications on the thermal stability of different G-quadruplexes-forming oligonucleotides. Nucleic Acids Res 33:1182–1192

Sen D, Gilbert W (1998) Formation of parallel four-stranded complexes by guanine-rich motifs in DNA and its implications for meiosis. Nature 344:410–444

Shammas MA, Reis RJS, Li C, Koley H, Hurley LH, Anderson KC, Munshi NC (2004) Telomerase inhibition and cell growth arrest after telomestatin treatment in multiple myeloma. Cancer Res 10:770–776

Spackova N, Berger I, Sponer J (1999) Nanosecond molecular dynamics simulation of parallel and antiparallel guanine quadruplex DNA molecules. J Am Chem Soc 121:5519–5534

Stelf R, Cheatham TE III, Spackova N, Fadrna E, Berger I, Koca J, Sponer J (2003) Formation pathways of a guanine-quadruplex DNA revealed by molecular dynamics and thermodynamic analysis of the substates. Biophys J 85:1787–1804

Tan JH, Gu LQ, Wu JY (2008) Design of selective G-quadruplex ligands as potential anticancer agents. Mini Rev Med Chem 8:1163–1178

Walsh K, Gualberto A (1992) MyoD binds to the guanine tetrad nucleic acid structure. J Biol Chem 267:13714–13718

Wang W, Chen HJ, Sun J, Benimetskaya L, Schwartz A, Cannon P, Stein CA, Rabbani LE (1998) A comparison of guanosine-quartet inhibitory effects versus cytidine homopolymer inhibitory effects on rat neointimal formation. Antisense Nucleic Acid Drug Dev 8:227–236

White JR, Gordon-Smith EC, Rutherford TR (1996) Phosphorothioate-capped antisense oligonucleotides to Ras GAP inhibit cell proliferation and trigger apoptosis but fail to downregulate GAP gene expression. Biochem Biophys Res Commun 227:118–124

Yang L, Tan C, Hsieh M, Wang J, Duan Y et al (2006) New-generation Amber united-atom force field. J Phys Chem B 110:13166–13176

Zimmerman SB, Cohen GH, Davies DR (1975) X-ray fiber diffraction and model-building study of polyguanylic acid and polyinosinic acid. J Mol Biol 92:181–184